第 38 卷第 3 期 分 子 催 化 (中 英 文) Vol.38,No.3
2024 年 6 月 JOURNAL OF MOLECULAR CATALYSIS(CHINA) Jun. 2024

Article ID：1001-3555(2024)03-0208-07 *Articles*

Nitrogen-Doped Ordered Mesoporous Carbon Supported Co Nanoparticles Catalyzed Hydrogenation of Aliphatic Amides

ZHENG Huan[1,2], GAO Wei[1], LIU Ze-bang[1*], HE Lin[1,2*]

(1. State Key Laboratory for Oxo Synthesis and Selective Oxidation, Lanzhou Institute of Chemical Physics, Chinese Academy of Sciences, Lanzhou 730000, China; 2. University of Chinese Academy of Sciences, Beijing 100049, China)

Abstract: Selective hydrogenation of amides is an attractive route for the production of amines. Traditional processes commonly used noble metal catalysts and high-pressure H_2, which are not cost-saving and selectivity-controllable. Nitrogen-doped ordered mesoporous carbon supported Co nanoparticles catalysts (Co/MNC) were prepared *via* an ion exchange-pyrolysis strategy, which showed good activity and selectivity in hydrogenation of aliphatic amides. It was found that the supported Co catalysts pyrolyzed at 500 ℃ possessed the uniform dispersion of Co nanoparticles and the co-existence of Co^0 and Lewis acidic CoO_x species, thus resulting in a boosted catalytic performance, which was more active than other counterparts as well as Co/MNC-600 and Co/MNC-700.

Key words: nitrogen-doped ordered mesoporous carbon; Co nanoparticles; hydrogenation; aliphatic amides

CLC number: O643.32 **Document code:** A **DOI:** 10.16084/j.issn1001-3555.2024.03.002

Aliphatic amines are widely applied in the production of pharmaceuticals, agrochemicals, surfactants, dyes and polymers[1−2]. Selective catalytic hydrogenation of amides to the corresponding amines using the hydrogen molecular is an environmentally friendly route as the only byproduct is water. However, the hydrogenation of amides is very challenging because of the resonance stabilization caused by a delocalization of the nitrogen electronic lone pair. In addition, the hydrogenation of amides always produces more by-products like alcohols and N-substituted products[3−4]. Therefore, it is a great challenge to develop efficient catalytic systems for hydrogenation of amides.

Homogeneous systems using metal complex and acidic or basic additives have been reported to be active for amide hydrogenation[5−9]. However, it is difficulty in the product separation and catalysts recycling. While heterogeneous catalysts can avoid such difficulties and are more suitable for industrial applications. Recently, heterogeneous noble metal catalytic systems have been extensively studied in amide hydrogenation. Bimetallic catalytic systems which consist of a noble metal and an oxophilic metal such as Rh-Mo[10], Rh-Re[11], Ru-Re[11], Pt-Re[12−13], Pt-V[14], Rh-V[15], Ru-W[16], Ru-Mo[17−19] and Ir-Mo[20] have been proved to be effective for amide hydrogenation. The use of precious metals will undoubtedly increase the cost for the hydrogenation process. And heterogeneous non-noble catalysts for amide hydrogenation were rarely reported. Shen *et al*. prepared 60%Ni/LaAlSiO catalysts for the hydrodeoxygenation of *N,N*-dimethylformamide (DMF) to trimethylamine (TMA) in a fixed-bed reactor in 2016[21]. Hu *et al*. recently reported that NiMo nitrides catalysts can facilitate the hydrogenation of aliphatic acyclic amides under the mixed atmosphere of H_2 and NH_3[22]. In conclusion, the development of efficient non-noble heterogeneous catalysts which allow for selective hydrogenation of amides is still highly demanded.

It has been reported that heterogeneous cobalt-based catalysts such as reduced Co_3O_4 or *N*-doped carbon supported Co catalysts have a strong ability to activate the C═O bonds in the hydrodeoxygenation of biomass-derived compounds[23−26]. And the activity depends on the reducibility and dispersion of supported cobalt. We anticipate that the supported Co catalysts may be also applicable for the hydrogenation of aliphatic amides to amines. In this work, the nitrogen-doped ordered mesoporous carbon supported Co nanoparticles (Co/MNC) were prepared *via* an ion exchange-pyrolysis strategy[27]. The supported Co catalysts pyrolyzed at 500 ℃ possessed the uniform dispersion of Co nanoparticles and the co-existence of Co^0 and Lewis acidic CoO_x species, showed good catalytic activity and selectivity in hydrogenation of aliphatic amides, affording a maximum yield of cyclohexylmethylamine to 70.6% at 180 ℃ under 3 MPa H_2. Moreover, this catalytic system was available to primary, secondary and tertiary aliphatic amides.

1 Experimental Section

1.1 Catalyst preparation

Mesoporous nitrogen-doped carbon (MNC) was prepared according to the literature [27]. Generally, 3.08 g of 2,4-dihydroxybenzoic acid, 0.6 g of ethylenediamine, 0.934 g of hexamethylenetetramine and 3.5 g of P123 were dissolved in 80 mL of deionized water. And the mixed solution was stirred at room temperature for 2 h. Then, the above solution was transferred into a Teflon-lined stainless-steel autoclave. After keeping at 130 ℃ for 4 h, the autoclave was cooled down to

Received date: 2024-03-04; **Revised date:** 2024-04-05.
Foundation: The Natural Science Foundation of Jiangsu Province (No. BK20211094).
Biography: Zheng Huan(1993−), male, master, engaged in the research of heterogeneous catalytic hydrogenation. E-mail: zhenghuan19@mails.ucas.ac.cn.
* Corresponding authors. E-mail: liuvca@126.com; helin@licp.cas.cn.

room temperature, and the obtained orange-red polymer gel was washed three times with deionized water.

Nitrogen-doped ordered mesoporous carbon supported Co nanoparticles were prepared through an ion exchange-pyrolysis strategy[27−28]. Typically, the orange-red polymer was first prepared according to the above-suggested method and was redispersed in a mixture of 96 mL of H_2O and 24 mL of ammonium hydroxide solution (28.0%~30.0%), followed by the addition of 1.345 g of $Co(NO_3)_2·6H_2O$. After stirring at 50 ℃ for 6 h, the suspension was centrifuged, and a brown solid was obtained after washing the precipitate with deionized water three times and drying at 50 ℃ under vacuum for 8 h. Then, the brown solid was treated under a H_2/N_2 (5%/95%) atmosphere at different temperatures for 2 h with a heating rate of 2 ℃·min^{-1}. After that, 1% O_2/Ar was introduced to passivate the surface of catalysts. The obtained samples were labeled as Co/MNC-T, in which T indicates the reduction temperature. Cu/MNC and Ni/MNC were obtained through the similar preparation process when using $Cu(NO_3)_2·6H_2O$ and $Ni(NO_3)_2·6H_2O$ as the metal precursor.

1.2 Catalyst characterization

The X-ray powder diffraction (XRD) patterns were obtained by using a D8 ADVANCE X-ray with Cu Kα radiation (λ=0.154 05 nm). Transmission electron microscopy (TEM) was characterized on a JEOL 2100 electron microscope operated at 200 kV. Nitrogen adsorption-desorption isotherms were measured at −196 ℃ using a Micromeritics ASAP 2460 analyzer. The specific surface areas were calculated according to the Brunauer-Emmet-Teller (BET) method. The pore size distribution was determined by Barret-Joyner-Halenda (BJH) model. X-ray photoelectron spectroscopy (XPS) measurements were recorded on a Thermo Scientific K-Alpha working in the constant analyzer energy mode with Al Kα radiation as the excitation source. The carbonaceous C 1*s* line (284.8 eV) was used as the reference to calibrate the binding energies (B.E.). Fourier-transform infrared (FT-IR) experiments were conducted on Thermo Scientific Nicolet-iS50 FT-IR spectrometer, and the Raman spectra were carried out on Thermo Scientific DXR 3Xi with a 532 nm excitation wavelength. Inductively coupled plasma-Mass Spectrometry (ICP-MS) was conducted on NexION 350X.

1.3 Catalytic test

In a typical reaction, 50 mg of catalyst, 0.5 mmol of substrate and 3 mL solvent was added in a 10 mL high-pressure stainless-steel autoclave and purged with H_2 for three times at room temperature. After the autoclave was purged with H_2 to desired pressure, it was heated to 180 ℃ for 12 h. It was then let to cool down to room temperature and depressurized, and the reaction medium was centrifuged. Conversions and yields were determined by GC with dodecane as an internal standard. The GC sensibility was calibrated using the commercial products. The amide conversion (Conv.) and product selectivity (Sel.) were calculated with the follow equations:

$$\text{Conv.}(\%,\ \text{amide}) = \frac{n(\text{amide consumed})}{n(\text{amide fed})} \times 100$$

$$\text{Sel.}(\%,\ \text{CyCH}_2\text{NH}_2) = \frac{n(\text{CyCH}_2\text{NH}_2\ \text{produced})}{n(\text{amide consumed})} \times 100$$

$$\text{Sel.}(\%,\ \text{CyCH}_2\text{OH}) = \frac{n(\text{CyCH}_2\text{OH produced})}{n(\text{amide consumed})} \times 100$$

$$\text{Sel.}(\%,\ (\text{CyCH}_2)_2\text{NH}) = 2 \times \frac{n((\text{CyCH}_2)_2\text{NH produced})}{n(\text{amide consumed})} \times 100$$

$$\text{Sel.}(\%, \text{Others}) = 100 - \text{Sel.}(\%, \text{CyCH}_2\text{NH}_2) - \text{Sel.}(\%, \text{CyCH}_2\text{OH}) - \text{Sel.}(\%, (\text{CyCH}_2)_2\text{NH})$$

2 Results and Discussion

Co/MNC-T was prepared by an ion exchange process, followed by pyrolysis for removing P123 and reducing cobalt partially (Fig. 1(a)). The structure of Co/MNC-T samples were characterized by X-ray diffraction (XRD). As for all samples, a board peak at 22° could be ascribed to C(002) diffraction (Fig.1(b)). On increasing the temperature from 500 to 700 ℃, the diffraction of Co(111) strengthened gradually, probably ascribing to the increased particle size. Subsequently, the nitrogen adsorption–desorption measurements for the Co/MNC samples were conducted to determine the pore structure and surface area. As shown in Fig.1(c), the N_2 adsorption/desorption isotherms of all samples could be considered as type Ⅳ plots with a type H3 hysteresis loop starting from about P/P_0 = 0.45, indicating the samples have mesopores. The pore size distribution curve (Fig.1(d)) further demonstrated the dominant presence of mesoporous in these samples. The surface areas and pore sizes and volumes are summarized in Table 1. The BET surface area of the Co/MNC-500 is 464 m^2·g^{-1} and the pore volume is 0.33 cm^3·g^{-1}. As the pyrolysis temperature increased, both the surface areas and pore volumes slightly decreased. The reason for the decrease of the surface area might be due to the partial collapse of the mesoporous structure under an extra high heating temperature.

Transmission electron microscopy (TEM) studies were carried out to investigate the morphology and particle size. The TEM image of the Co/MNC-500 sample showed uniform nanoparticles with an average size of about 3.30 nm on the support (Fig.1(j)). To identify whether the nanoparticles belong to certain Co species, a high-resolution TEM analysis (HR-TEM) of Co/MNC-500 was conducted. As shown in Fig.1(k), two distinct lattice planes with the lattice spacing of 0.203 and 0.213 nm, which could be ascribed to the Co(111) and CoO(200) planes, indicating that the co-existence of CoO and Co^0. The scanning TEM (STEM) image and the corresponding energy-dispersive X-ray (EDX) elemental mapping images of the Co/MNC-500 sample are shown in Fig.1(f)−(i). The images clearly illustrated the uniform distribution of C, N, O, and Co elements on the sample. The Fig.1(j)−(o) showed that the average nanoparticle size increased with the enhanced pyrolysis temperature due to the aggregation of Co nanoparticles at higher pyrolysis temperature.

FT-IR measurements were carried out to check the functional groups present on the sample surface. The spectra of Co/MNC-T are displayed in Fig. 2(a). Both samples contained broad peaks with varying intensities at around 3 420 cm^{-1}, which could be assigned to the O—H stretching vibration. The stretching of the C═N group for both samples appeared at 1 590cm^{-1}. Raman spectroscopy was used to further investigate the graphitic character of the samples. As shown in Fig. 2(b),

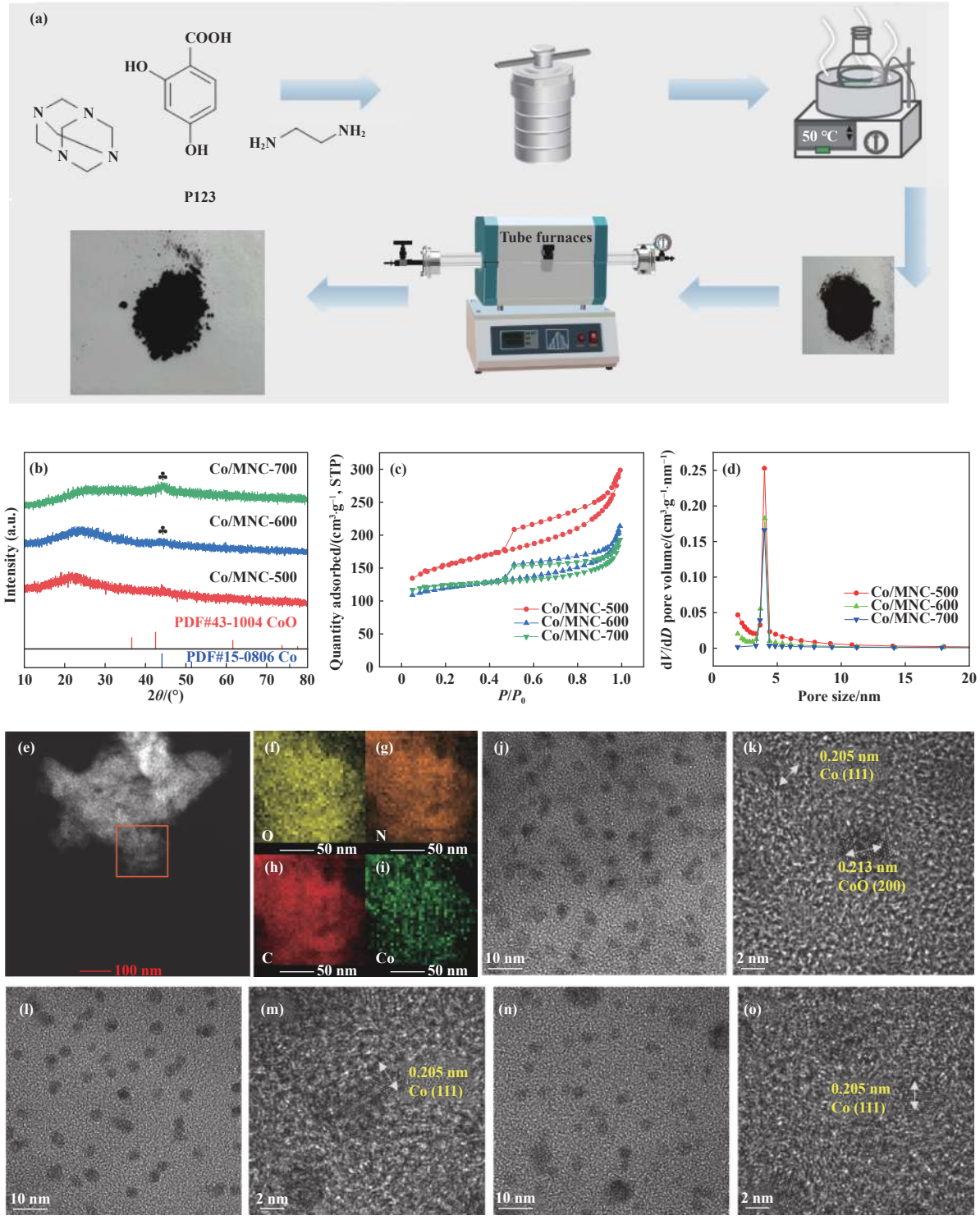

Fig.1 (a) Schematic illustration of the preparation of Co/MNC; (b) XRD image; (c) Nitrogen adsorption-desorption curves; (d) pore size-distribution of Co/MNC; (e) STEM image; (f)−(i) corresponding elemental mapping images of Co/MNC-500, HR-TEM images of (j)−(k) Co/MNC-500; (l)−(m) Co/MNC-600; (n)−(o) Co/MNC-700

two intense peaks appeared at 1 369 and 1 600 cm^{-1} for all samples which are assigned to the D band (defects in carbon matrix) and G band (in-plane stretching vibration of sp^2 hybridization of C atoms). For Co/MNC-T samples, the I_D/I_G ratio calculated based on the peak area are 0.66~0.76, demonstrating that higher pyrolysis temperature might lead to more defects. Furthermore, XPS was carried out to explore the elemental state of the series of catalysts. As shown in Fig. 2(c), Co 2*p* spectra are fitted into four peaks at 778.8, 780.5, 782.5, and 786.7 eV, which belong to Co^0, Co^{3+}, Co^{2+}, and satellite peaks, respectively[28−30]. The proportions of Co species in each catalyst are shown in Table 2. With the enhanced pyrolysis

Table 1 Characteristics of Co/MNC-T catalysts

Catalyst	S_{BET} /($m^2 \cdot g^{-1}$)	Pore volume /($cm^3 \cdot g^{-1}$)	Pore size /nm	Mass fraction/%					Particle size[c] /nm
				C[a]	N[a]	H[a]	O	Co[b]	
Co/MNC-500	464	0.33	5.4	61.4	3.1	2.4	22.2	10.9	3.30
Co/MNC-600	394	0.21	6.0	66.0	2.5	1.8	17.6	12.1	3.57
Co/MNC-700	361	0.14	7.3	66.1	1.6	1.1	17.7	13.5	3.92

a. Measured by elemental analysis;

b. Measured by ICP-MS;

c. As determined *via* TEM

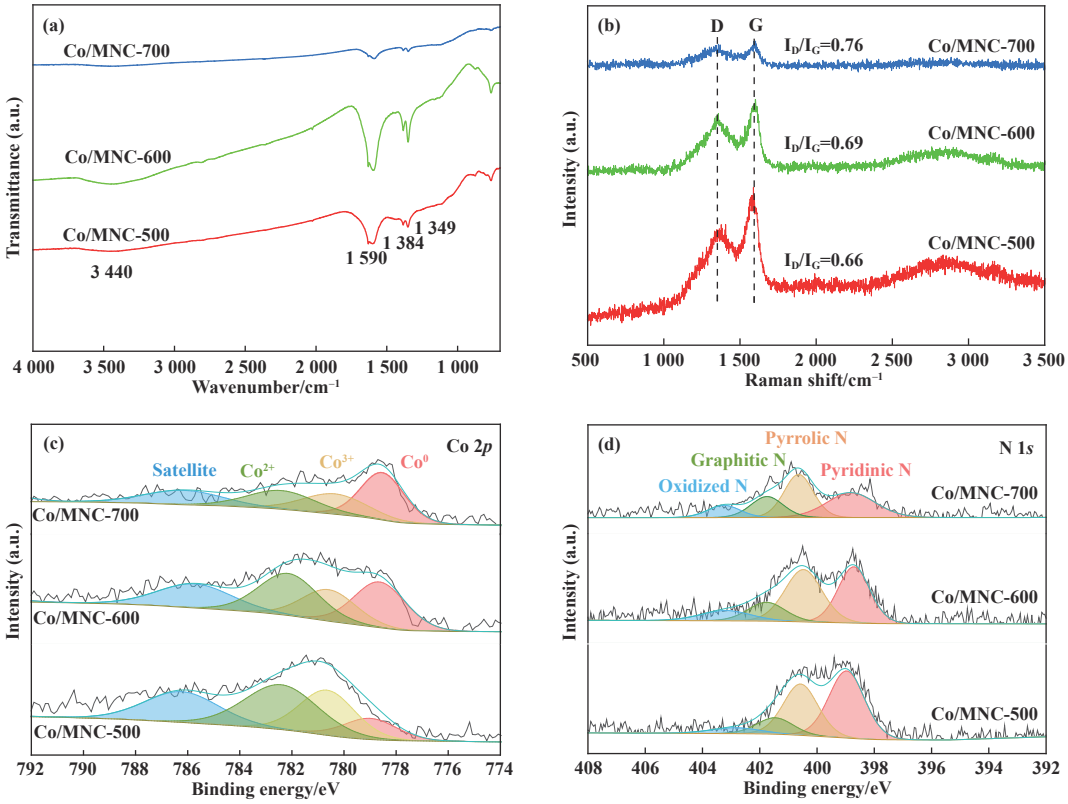

Fig.2 (a) FT-IR spectra; (b) Raman spectra; (c) Co 2*p*; (d) N 1*s* spectra of Co/MNC-500, Co/MNC-600 and Co/MNC-700

Table 2 Relative abundance ratio of N species and Co species on Co/MNC catalysts

Catalyst	Co species molar ratio[a] /%				N species molar ratio[a] /%			
	Co^0	Co^{3+}	Co^{2+}	Satellite	Pyridinic-N	Pyrrolic-N	Graphitic-N	NO
Co/MNC-500	12.1	27.1	35.8	25.0	47.4	35.1	11.8	5.7
Co/MNC-600	28.3	22.3	28.0	21.4	40.9	38.0	13.6	7.5
Co/MNC-700	35.9	20.6	24.0	19.5	34.1	35.4	19.2	11.3

a. Calculated by the relative area

temperature, the proportion of Co^{3+} and Co^{2+} decreased, while the proportion of Co^0 increased. Four peaks of N 1*s* are observed at 398.5, 400.0, 401.0, and 403.0 eV (Fig. 2(d)), which belong to pyridinic N, pyrrolic N, graphitic N, and NO, respectively. The relative abundance ratio of pyridinic N was decreased obviously as the pyrolysis temperature increased. Based on the above results, cobalt species were reduced during the pyrolysis process, thus resulting in the co-existence of Co^0 and Lewis acidic CoO_x species on the surface of catalysts.

As shown in Table 3, the above Co/MNC catalysts

Table 3 Hydrogenation of *N*-acetylmorpholine over various catalysts[a)]

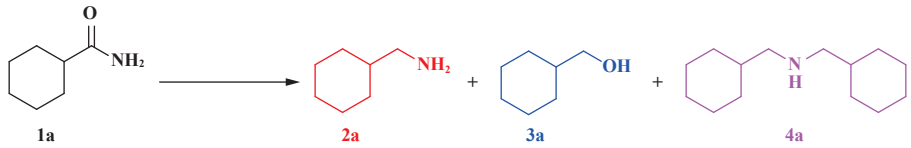

Entry	Catalysts	Conv./%	Sel./%				Yield/%
			2a	3a	4a	Others[b)]	
1	Co/MNC-400	–	–	–	–	–	–
2	Co/MNC-500	92.4	76.5	3.3	18.5	1.7	70.6
3	Co/MNC-600	58.6	73.8	–	20.9	5.3	43.2
4	Co/MNC-700	10.5	–	–	89.7	10.3	–
5	Cu/MNC-500	–	–	–	–	–	–
6	Ni/MNC-500	–	–	–	–	–	–

a) Reaction condition: Catalyst 50 mg, CPME 3 mL, $CyCONH_2$ 0.5 mmol, 180 ℃, H_2 3.0 MPa, 12 h;

b) Representing loss of carbon balance predominantly *via* formation of solid products on the catalyst surface.

were investigated for the hydrogenation of amides. Cyclohexanecarboxamide ($CyCONH_2$, **1a** was chosen as a representative substrate for primary amides, and all the catalysts were evaluated at 180 °C and 3 MPa H_2. Cu/MNC and Ni/MNC were also prepared for the hydrogenation of amides. However, these two catalysts showed no activity towards the reaction. It is shown that Co/MNC-500 exhibits the best catalytic performance among all the investigated catalysts, with 92.4% conversion of $CyCONH_2$ and 76.5% selectivity of $CyCH_2NH_2$. However, further increasing the pyrolysis temperature resulted in 58.6% $CyCONH_2$ conversion for Co/MNC-600. These results indicate that the pyrolysis temperature plays a key role in $CyCONH_2$ hydrogenation to $CyCH_2NH_2$. Combined with results of TEM and XPS (Fig. 1(e)−(o), Fig. 2(d)), we conclude that uniform small size of Co nanoparticles and an appropriate ratio of Co^0 and Lewis acidic CoO_x species are important for the hydrogenation of amides.

Since the Co/MNC-500 catalyst gave rise to the highest activity and selectivity, we then investigated the reaction stability and substrate applicability. As shown in Fig. 3(a), the conversion was around 92.4% and the selectivity to $CyCH_2NH_2$ was 76.5% for the first runs. However, the conversion decreased to 30.9% for the second runs. The loss of catalytic activity occurred to some extent during the repeated runs. When the spent catalyst was thermal treated in 5% H_2/N_2 at 500 ℃ for 1 h, the $CyCONH_2$ conversion recovered to 91.6%, indicating that the spent Co/MNC-500 could be regenerated through such a simple and reduction process. The Co leaching experiments were also investigated by ICP-MS. After each reaction, the content of Co in the filtrate was less than 1 $mg \cdot L^{-1}$. Form the TEM pattern of reused Co/MNC-500 catalyst (Fig. 3(b)), there is no obvious change about the particle size of Co nanoparticles, indicating the catalyst was stable during the reaction. In addition, it exhibited good activity and selectivity for a variety of primary, secondary and tertiary amides to the corresponding amines (Table 4).

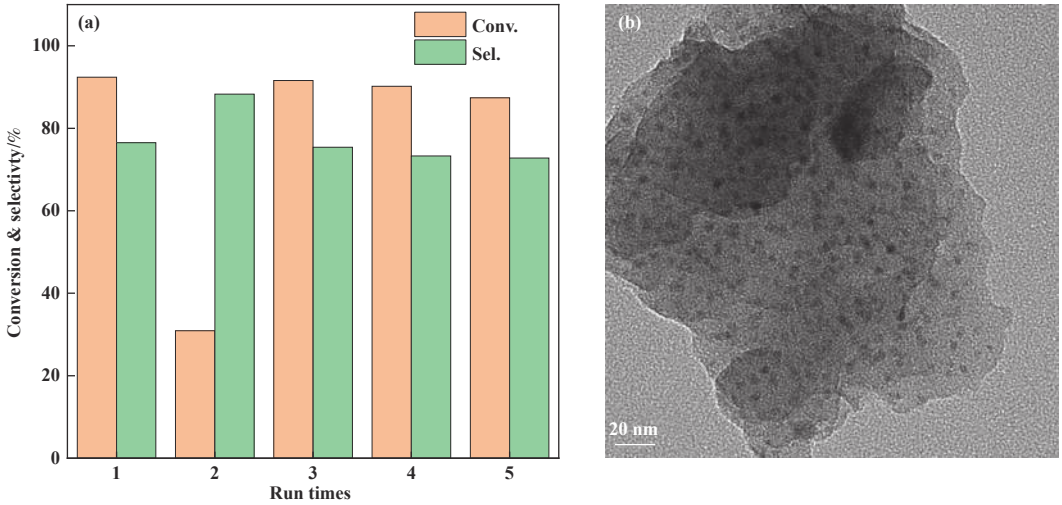

Fig.3 (a) Reusability test of Co/MNC-500 catalyst in hydrogenation of $CyCONH_2$; (b) TEM pattern of reused Co/MNC-500 catalyst; Reaction condition: Co/MNC-500 50 mg, CPME 3 mL, $CyCONH_2$ 0.5 mmol, 180 ℃, H_2 3.0 MPa, 12 h

Table 4 Controllable catalytic hydrogenation of various amides to corresponding amines over Co/MNC-500[a]

Entry	Substrate	Product	Conv. /%	Sel./%	Yield/%
1	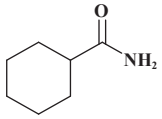	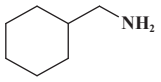	92.4	76.5	70.6
2	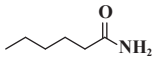		97.3	80.6	78.6
3	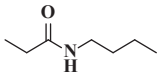		100	84.2	84.2
4	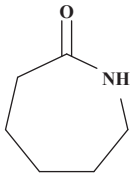	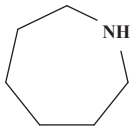	100	92.5	92.5
5	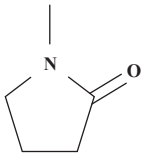	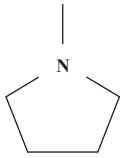	48.7	82.6	40.2
6	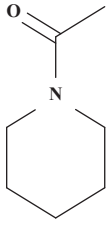	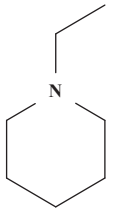	83.7	87.4	73.2
7	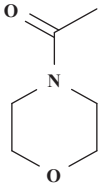	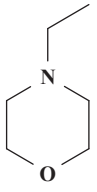	85.0	88.1	75.0

a. Reaction condition: Co/MNC-500 50 mg, CPME 3 mL, substrate 0.5 mmol, 180 ℃, H_2 3.0 MPa, 12 h

3 Conclusion

Efficient nitrogen-doped ordered mesoporous carbon supported Co nanoparticles were prepared *via* an ion-exchange and pyrolysis strategy for the hydrogenation of amides. The optimal pyrolysis temperature of 500 ℃ under hydrogen atmosphere was found to result in the highest activity and selectivity, while both Co/MNC-600 and Co/MNC-700 were not efficient for amide conversion. Characterization showed that the suitable pyrolysis temperature could lead to uniform dispersion of small Co nanoparticles and the co-existence of both the Co^0 and Lewis acidic CoO_x species over Co/MNC. The synergy between two cobalt species was responsible for the high reactivity of Co/MNC-500 in the hydrogenation of aliphatic amides.

References

[1] a. Smith A M, Whyman R. Review of methods for the catalytic hydrogenation of carboxamides[J]. *Chem Rev*, 2014, **114**(10): 5477−5510.

b. Li Y D, Li Y, Xia C G, *et al*. Recent advances in manganese-catalyzed hydrogenation reactions[J]. *J Mol Catal (China)*, 2022, **36**(1): 71−80.

[2] Formenti D, Ferretti F, Scharnagl F K, *et al*. Reduction of nitro compounds using 3*d*-non-noble metal catalysts[J]. *Chem Rev*, 2019, **119**(4): 2611−2680.

[3] Toyao T, Siddiki S M A H, Kon K, *et al*. The catalytic reduction of carboxylic acid derivatives and CO_2 by metal nanoparticles on Lewis-Acidic supports[J]. *Chem Rec*, 2018, **18**(10): 1374−1393.

[4] Cabrero-Antonino J R, Adam R, Papa V, *et al*. Homogeneous and heterogeneous catalytic reduction of amides and related compounds using molecular hydrogen[J]. *Nat Commun*, 2020, **11**(1): 3893.

[5] Ravn A K, Rezayee N M. The investigation of a switchable iridium catalyst for the hydrogenation of amides: A case study of C—O versus C—N bond scission[J]. *ACS Catal*, 2022, **12**(19): 11927−11933.

[6] a. Yuan M L, Xie J H, Zhu S F, *et al*. Deoxygenative hydrogenation of amides catalyzed by a well-defined iridium pincer complex[J]. *ACS Catal*, 2016, **6**(6): 3665−3669.

b. Nie C, Liu Q, Gao G, *et al*. Mesoporous carbon supported highly dispersed Fe-P catalyst for nitrobenzene hydrogenation[J]. *J Mol Catal (China)*, 2022, **36**(4): 330−337.

[7] Westhues S, Meuresch M, Klankermayer J. Ruthenium-catalyzed modular synthesis of cyclic tertiary amines from lactams[J]. *Angew Chem Int Ed*, 2016, **55**(41): 12841−12844.

[8] Garg J A, Chakraborty S, Ben-David Y, *et al*. Unprecedented iron-catalyzed selective hydrogenation of activated amides to amines and alcohols[J]. *Chem Commun*, 2016, **52**(30): 5285−5288.
[9] Meuresch M, Westhues S, Leitner W, *et al*. Tailor-made ruthenium-triphos catalysts for the selective homogeneous hydrogenation of lactams[J]. *Angew Chem Int Ed*, 2016, **55**(4): 1392−1395.
[10] Beamson G, Papworth A J, Philipps C, *et al*. Selective hydrogenation of amides using Rh/Mo catalysts[J]. *J Catal*, 2010, **269**(1): 93−102.
[11] Beamson G, Papworth A J, Philipps C, *et al*. Selective hydrogenation of amides using bimetallic Ru/Re and Rh/Re catalysts[J]. *J Catal*, 2011, **278**(2): 228−238.
[12] Stein M, Breit B. Catalytic hydrogenation of amides to amines under mild conditions[J]. *Angew Chem Int Ed*, 2013, **52**(8): 2231−2234.
[13] Burch R, Paun C, Cao X M, *et al*. Catalytic hydrogenation of tertiary amides at low temperatures and pressures using bimetallic Pt/Re-based catalysts[J]. *J Catal*, 2011, **283**(1): 89−97.
[14] Mitsudome T, Miyagawa K, Maeno Z, *et al*. Mild hydrogenation of amides to amines over a platinum-vanadium bimetallic catalyst[J]. *Angew Chem Int Ed*, 2017, **56**(32): 9381−9385.
[15] Pennetier A, Hernandez W Y, Kusema B T, *et al*. Efficient hydrogenation of aliphatic amides to amines over vanadium-modified rhodium supported catalyst[J]. *Appl Catal A -Gen*, 2021, **624**: 118301.
[16] Zhang Y, Li L, Liu F, *et al*. Synergy between Ru and WO_x enables efficient hydrodeoxygenation of primary amides to amines[J]. *ACS Catal*, 2022, **12**(11): 6302−6312.
[17] Zhang Y, Zhang F, Li L, *et al*. Highly chemoselective reduction of amides to amines over a ruthenium−molybdenum bimetallic catalyst[J]. *ChemistrySelect*, 2022, **7**(37): e202203030.
[18] Zhang Y, Zhang F, Li L, *et al*. Decoration of Ru nanoparticles with mononuclear MoO_x boosts the hydrodeoxygenation of amides to amines[J]. *J Catal*, 2023, **417**: 301−313.
[19] Beamson G, Papworth A J, Philipps C, *et al*. Selective hydrogenation of amides using ruthenium/molybdenum catalysts[J]. *Adv Synth Catal*, 2010, **352**(5): 869−883.
[20] Chen T, Shi Z, Zhang G, *et al*. Molybdenum-incorporated mesoporous silica: Surface engineering toward enhanced metal-support interactions and efficient hydrogenation[J]. *ACS Appl Mater Interfaces*, 2018, **10**(49): 42475−42483.
[21] Li S, Chen H, Wen M, *et al*. Preparation of hydrothermally stable, basic, and highly active nano nickel catalysts for the hydrodeoxygenation of *N,N*-dimethylformamide[J]. *J Catal*, 2016, **338**: 1−11.
[22] Yang H, Zhou L, Chen H, *et al*. Efficient hydrogenation of aliphatic acyclic amides to amines by bimetallic NiMo nitrides *via* heterogeneous catalysis[J]. *Chem Eng J*, 2023, **473**: 145374.
[23] Li D, Liu Q, Zhu C, *et al*. Selective hydrogenolysis of 5-hydroxymethylfurfural to 2,5-dimethylfuran over Co_3O_4 catalyst by controlled reduction[J]. *J Energy Chem*, 2019, **30**: 34−41.
[24] Xiang S, Dong L, Wang Z Q, *et al*. A unique Co@CoO catalyst for hydrogenolysis of biomass-derived 5-hydroxymethylfurfural to 2,5-dimethylfuran[J]. *Nat Commun*, 2022, **13**(1): 3657.
[25] Li X L, Zhang K, Chen S Y, *et al*. A cobalt catalyst for reductive etherification of 5-hydroxymethyl-furfural to 2,5-bis(methoxymethyl)furan under mild conditions[J]. *Green Chem*, 2018, **20**: 1095−1105.
[26] Liu X, Xu L, Xu G, *et al*. Selective Hydrodeoxygenation of lignin-derived phenols to cyclohexanols or cyclohexanes over magnetic CoN_x@NC catalysts under mild conditions[J]. *ACS Catal*, 2016, **6**(11): 7611−7620.
[27] Wang G H, Deng X, Gu D, *et al*. Co_3O_4 Nanoparticles supported on mesoporous carbon for selective transfer hydrogenation of alpha, beta-unsaturated aldehydes[J]. *Angew Chem Int Ed*, 2016, **55**(37): 11101−11105.
[28] Nie Y, Lin W, Zhang Y, *et al*. Transfer hydrogenation of phenol over Co-CoO_x/N-doped carbon: Boosted catalyst performance enabled by synergistic catalysis between Co^0 and Co^{δ}[J]. *Dalton Trans*, 2022, **51**(41): 15983−15989.
[29] Yang H, Chen H, Zhou W, *et al*. Construction of N, O co-doped carbon anchored with Co nanoparticles as efficient catalyst for furfural hydrodeoxygenation in ethanol[J]. *J Energy Chem*, 2023, **78**: 195−202.
[30] Lu X, Qin J, Xian C, *et al*. Cobalt nanoparticles supported on microporous nitrogen-doped carbon for an efficient catalytic transfer hydrogenation reaction between nitroarenes and *N*-heterocycles[J]. *Catal Sci Technol*, 2022, **12**(18): 5549−5558.

氮掺杂的有序介孔碳负载钴纳米颗粒用于脂肪酰胺的催化加氢

郑 欢[1,2], 高 玮[1], 刘泽邦[1*], 何 林[1,2*]

(1. 中国科学院兰州化学物理研究所 羰基合成与选择氧化国家重点实验室, 甘肃 兰州 730000;
2. 中国科学院大学, 北京 100049)

摘要: 酰胺的选择性加氢可以作为有机胺的一种生产路径. 传统的酰胺加氢多相催化体系多采用贵金属催化剂和高压氢气, 存在成本较高的问题. 我们采用离子交换热解法制备了氮掺杂有序介孔碳负载钴纳米颗粒催化剂(Co/MNC), 该催化剂在脂肪族酰胺加氢反应中表现出良好的活性和选择性. 结果表明, 负载型 Co 催化剂在 500 ℃下热解后, Co 纳米颗粒分散均匀, 催化剂表面同时存在金属 Co^0 和具有路易斯酸性的 CoO_x, 催化性能明显优于 Co/MNC-600 和 Co/MNC-700.

关键词: 氮掺杂有序介孔碳; 钴纳米颗粒; 加氢; 脂肪酰胺